# Developments of Multistep Inverse Finite Element Method and Its Application in Formability Prediction of Multistage Sheet Metal Forming

**Bingtao Tang**[1]
Institute of Engineering Mechanics,
Shandong Jianzhu University,
Jinan 250101, China;
State Key Laboratory of Materials Processing and
Die and Mould Technology,
Huazhong University of Science and Technology,
Wuhan 410082, China
e-mail: tbtsh@hotmail.com

**Yunjiang Li**

**Xiaoyang Lu**

Institute of Engineering Mechanics,
Shandong Jianzhu University,
Jinan, China

*In the paper, the multistep inverse finite element method (FEM) has been introduced to improve the accuracy of simulation in sheet metal stamping. Furthermore, the multistep inverse FEM can be used to obtain the strain/thickness distribution and shape of blank in the intermediate configurations. But there are three key problems, which are essential to implement multistep inverse FEM: the fist one is how to obtain the intermediate configurations of intermediate steps, the second one is how to find the corresponding Z coordinates in the sliding constraint surface, and the last one is how to update strain/stress distribution in the intermediate configurations in a fast and reliable way. Based on the known configurations of punch and die of the current step, the strategy of area minimization coupled with feasible sequential quadratic programming code is used to obtain initial intermediate configurations. An efficient walk-through point location algorithm with its complexity $O(n^{1/d})$ per point (d means the space dimension) is used to deal with contact searching problem and restrain the movement of corresponding nodes of intermediate configurations. In order to preserve the computational efficiency of inverse FEM, a pseudodeformation theory of plasticity based constitutive equation is proposed, which can well reflect the actual forming condition such as elastic/plastic deformation or loading/unloading condition. The above-mentioned improvements are implemented in our in-house inverse analysis software INVERSTAMP/MULTISTEP module. The presented algorithms are applied to a two-step cylinder cup deep-drawing product and three-step S-rail forming case. The numerical results compared with explicit dynamic solver LS-DYNA3D confirm its validity in formability prediction of intermediate shapes and final workpiece.*
[DOI: 10.1115/1.4001868]

*Keywords: sheet metal forming, inverse FEM, contact searching, constitutive equations, point location algorithm*

## 1 Introduction

A large number of parts on automobile body are deformed by stamping process. During the last decade, numerical simulation has been widely used to evaluate process and tool design as well as forming defects such as fracture and wrinkling [1]. Improvement of the design and tryout procedures using numerical simulations have a significant impact on the cost of the tools and on the reduction in the total time from design to manufacture with also the possibility to provide better solutions than those determined from purely experimental tryout procedures.

There are mainly two approaches for sheet metal forming simulation: an incremental approach and an inverse finite element method (FEM). For most of automobile industrial parts, incremental approach is time consuming and involves expensive computer resources while the inverse FEM is simple and very efficient. In the automobile industry, the two approaches are usually used at different design stage and are complemented to each other. The one-step inverse FEM is based on the knowledge of the final workpiece. The assumption of proportional loading and simplified tool actions lead to a "one-step" algorithm. With the known information of the final configuration, a Newton–Raphson resolution scheme is used to find the original node positions on the initial flat blank satisfying the equilibrium in the final configuration, thus, the strain and stress tensors are obtained. When the sheet metal is drawn over a die radius, the material is subjected to stretching-bending/unbending deformation, which strongly influences the sheet formability. In order to take into account the deformation history, some realistic intermediate configurations are determined and considered.

The multistep inverse FEM has been developed recently in order to consider the loading history and to improve the stress estimation in keeping the simplicity and efficiency of one-step inverse FEM. Based on the assumption of ideal forming theory and plain stress, Majlessi and Lee [2] formulated the FE equations for axisymetric multistep deep-drawing inverse FEM with linear membrane element and the rigid-plastic material model with no consideration of boundary conditions such as friction and blankholder forces. Lee and Cao [3] presented an axisymetric shell element for the multistep inverse FEM for more accurate prediction of the design variables, such as initial blank shape, strain distributions, intermediate shapes, etc., but their published paper was only restricted to axisymetric deep-drawing parts. Guo et al. [4] developed the pseudo-inverse approach, taking into account the loading history. 3D workpiece was divided into several

[1]Corresponding author.

Contributed by the Manufacturing Engineering Division of ASME for publication in the JOURNAL OF MANUFACTURING SCIENCE AND ENGINEERING. Manuscript received May 26, 2009; final manuscript received May 14, 2010; published online July 23, 2010. Assoc. Editor: Zhongqin Lin.

sectors, treated as 2D case in a sector and regrouped by linear interpolation. However, this approach was found to be very time consuming and to need expensive computer and human resources. They implanted the flow theory of plasticity into constitutive equation, which leads to a considerable improvement of the stress evaluation but relatively low computational efficiency. Lee and Huh [5] estimated shape and nonshape parameters in sheet metal forming for an oil pan and a front fender and suggested a linear mapping technique for the general three-dimensional multistage analysis and compared the result with the one-step analysis result. The principle of virtual work was adopted to get the equilibrium equations about initial nodal positions. Kim and Huh [6] used finite element inverse analysis approach to simulate multistage deep-drawing processes in order to calculate the thickness strain distribution in each intermediate shape and to design the intermediate die shapes. The concept of sliding constraint surface, which is needed to carry out the multistep analysis, was introduced and the corresponding procedure was also been described. The introduction of the sliding constraint surface and the adoption of three coordinate systems were relatively difficult to implement and was a time consuming task. Huang et al. [7] proposed a modified arc-length search method to obtain the initial solutions on the intermediate three-dimensional configurations by mapping the arc-length of the final part onto intermediate sliding constraint surfaces. It was efficient to solve simple deep-drawing examples, such as axisymetric multistep deep drawings, while it showed weak stability toward complex drawing cases. Tang et al. [8] proposed a double section curve expanding method to get initial solutions of intermediate configurations, which can take into account of plastic deformation characteristics. They also proposed a local and global combined searching scheme to restrain the moving of corresponding nodes but the double section curve expanding method showed its limitation when dealing with complicated stamping panels. The local and global combined searching scheme was also time consuming in this case.

In this paper, the authors first reviewed the assumptions and the main formulation of multistep inverse FEM including bending effects and then three developments are proposed to improve the reliability and efficiency of multistep inverse FEM:

## 2 Outlines of Multistep Inverse FEM

The traditional inverse FEM is based on the knowledge of the final workpiece. Its computation is carried out in one step by directly comparing the initial and final configurations with the results of node positions in the initial blank and the thickness and strain distributions in the final workpiece. However, a single-step approximation for a multistage forming process may not give a valid result. The multistep inverse FEM is developed from the basic idea of traditional one-step inverse FEM. The total strains on an intermediate configuration in the multistep inverse FEM are calculated in one step by directly comparing the initial flat blank and current intermediate contours. The strain increment between two successive configurations is obtained based on the relative displacement increment between them. In each step, the lower configuration is noted as the initial state and the adjacent higher one is noted as the final state. The node positions are updated in the initial state and other results, such as thickness and strain distribution, are updated in the final state.

The analysis is based on the idea of dividing the deformation history into several steps while applying the total strain theory of plasticity in each step. Suppose there are three configurations to be considered: initial flat blank $C^0$, curved intermediate, and final configurations $C^1$, C as shown in Fig. 1. Suppose $q$ is a material point on the final configuration, $q^1$ is the point on curved intermediate configuration, $q^0$ is the point on the initial flat blank correspondingly. Point $p$ is situated on the known sheet midsurface with the corresponding point on curved intermediate and initial flat configuration $p^1$ and $p^0$, respectively.

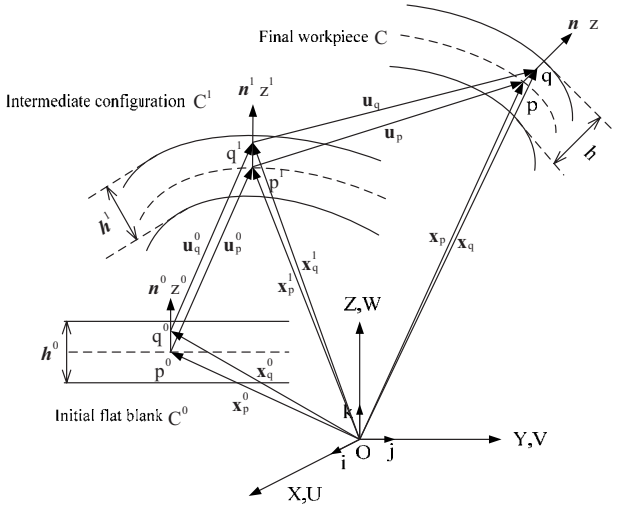


**Fig. 1 The kinematics relations of a thin shell model with intermediate configuration**

Position vector of node $q$ in the thickness is expressed as follows:

$$\boldsymbol{x}_q = \boldsymbol{x}_p + z\boldsymbol{n} \tag{1}$$

Introducing two unit orthogonal tangent vectors $\boldsymbol{t}_1$ and $\boldsymbol{t}_2$ onto the curved deformed middle surface as local curvilinear coordinates, then,

$$\mathrm{d}\boldsymbol{x}_q = (\boldsymbol{t}_1 + z\boldsymbol{n}_{p,x})\mathrm{d}x + (\boldsymbol{t}_2 + z\boldsymbol{n}_{p,y})\mathrm{d}y + \boldsymbol{n}\mathrm{d}z \tag{2}$$

The kinematic equation of a material point on the intermediate surface can be written as

$$\boldsymbol{x}_q^1 = \boldsymbol{x}_p - \boldsymbol{u}_p + z^1\boldsymbol{n}^1 \tag{3}$$

with $\boldsymbol{u}$ the vector displacement, thus,

$$\mathrm{d}\boldsymbol{x}_q^1 = (\boldsymbol{t}_1 - \boldsymbol{u}_{p,x})\mathrm{d}x + (\boldsymbol{t}_2 - \boldsymbol{u}_{p,y})\mathrm{d}y + \frac{\boldsymbol{n}^1}{\lambda_3}\mathrm{d}z \tag{4}$$

Translate into matrix form

$$d\boldsymbol{x}_q^1 = [F_x^1]^{-1}d\boldsymbol{x} \tag{5}$$

with

$$[F_x^1]^{-1} = \begin{bmatrix} \boldsymbol{t}_1 - \boldsymbol{u}_{p,x} & \boldsymbol{t}_2 - \boldsymbol{u}_{p,y} & \dfrac{\boldsymbol{n}^1}{\lambda_3} \end{bmatrix} \tag{6}$$

After further deduction, the inverse deformation gradient tensor $[F]^{-1}$ of point $q$ toward point $q^1$ is the same as that of point $q$ toward point $q^0$. The elastoplastic deformation is assumed to be independent of the loading path. The eigenvalue calculation and the incompressibility assumption allow obtaining the three principal stretches and the logarithmic strains. The Hencky–Ilyushin deformation theory of plasticity is employed for the calculation of Cauchy stress in the present displacement-based finite element analysis with given strain. In one-step inverse FEM, the displacement of node in vertical direction is known and remains constant during whole Newton–Raphson iterations. However, in multistep inverse FEM, the intermediate constraint surface is a three-dimensional part and the solution must be converged onto the surface $Z=f(X,Y)$, which means the vertical displacement of node is changeable with its horizontal movement.

## 3 Key Issues in Multistep Inverse FEM

**3.1 Generation of Intermediate Configurations.** In one-step inverse FEM, only the initial solution of the flat blank is needed during the whole procedure. However, in multistep inverse FEM,

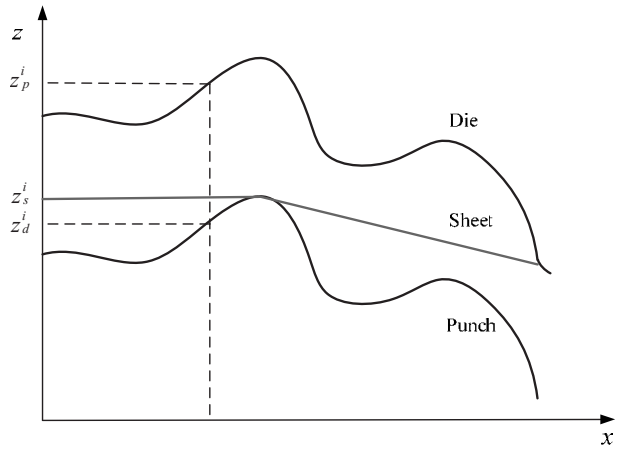


**Fig. 2 Generation of intermediate sheet configuration with known die and punch profiles**

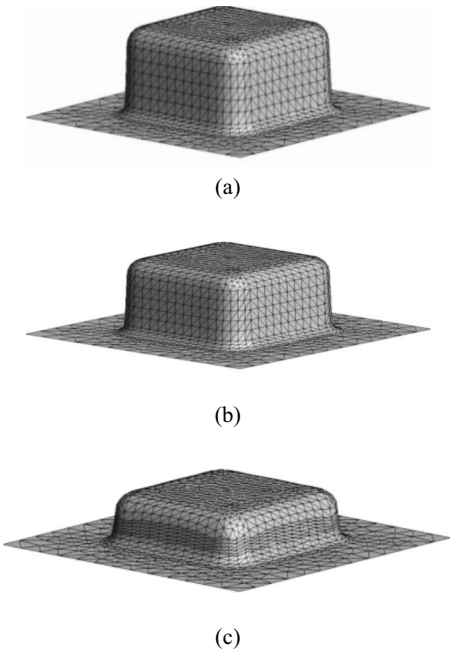


**Fig. 3 Two mesh system of final and intermediate configuration: (*a*) 40 mm punch travel, (*b*) 30 mm punch travel, and (*c*) 20 mm punch travel**

not only is the initial solution of the flat blank needed, but also, the initial solutions of intermediate configurations and the intermediate constraint surfaces are needed for the iteration solution to consider the deformation paths. As the shape of the tools and their positions are known during the forming process, a geometrical method can be used to generate the initial intermediate configurations.

Suppose a thin sheet metal is constrained between the punch and die and tensioned as a membrane in agreement with the tools geometrically (Fig. 2). For the deformation of most of automobile panels are mainly stretching, this simplification sounds reasonable [4]. The information of the die can be easily obtained by the known discretized final workpiece. Mesh under binder is separated and the remaining mesh is moved along $Z$ direction to be defined as punch. The contours of intermediate configurations can be determined by the minimization of area of the surfaces. The object function and the corresponding constraint condition are as follows:

$$J = \mathrm{Min} \sum_e A_e$$

$$z_p^i \le z_s^i \le z_d^i \tag{7}$$

where $A_e$ is area of an element surface, $z_p^i$, $z_s^i$, and $z_d^i$ represent the vertical coordinates of the nodes of the punch, sheet, and die, respectively, and $z_s^i$ are the design variables.

A generalization of Newton's method named sequential quadratic programming is used to solve this minimization problem. Figure 3(*a*) is the known final workpiece with 40 mm drawing depth. The intermediate configurations with punch travels of 30 mm and 20 mm are shown in Figs. 3(*b*) and 3(*c*). The present method gives intermediate meshes independent each other, that is to say, the nodes having the same number in different meshes do not represent the same material point. This problem can be overcome by the relocalization of the nodes on the geometrical mesh [4].

**3.2 Constraint Strategies on Sliding Constraint Surfaces.** In the one-step inverse FEM, the flat plane is the constraint surface for the update and convergence of initial flat blank. Likewise, the sliding constraint surface is introduced to guide the movement of nodes on intermediate configurations in the multistep FEM. The shape and position of the current die face serve as the sliding constraint surface. The initial displacement of node can be obtained with the initial solution obtained in the previous section. However, the node position after displacement increment should also satisfy the expression of constraint surface. The problem becomes, how to find the corresponding point on the sliding constraint surface in each iteration and obtain the vertical displacement of the specified node.

Figure 4 shows the update of node position from point $P$ to point $Q$ on the constraint surface with the displacement increment along $X$ and $Y$ directions $\Delta U_P^i$ and $\Delta V_P^i$, respectively. Points $M$ and $N$ are the projected points of points $P$ and $Q$ on $XOY$ plane, respectively. At step $i$, the node with initial displacements $U_P^i$ and $V_P^i$ will be converged to another position on the constraint surface (in Fig. 4, the corresponding point is $Q$).

$$U_P^{i+1} = U_P^i + \Delta U_P^i$$

$$V_P^{i+1} = V_P^i + \Delta V_P^i \tag{8}$$

In order to determine $W_P^{i+1}$ along $Z$ direction, the location of point $Q$ should be first decided. After finding the element that point $Q$ belongs to, its $Z$ coordinate is readily obtained using linear interpolation by the node coordinates of the element. But how to determine the node position on the three-dimensional discretized mesh in a short time is still a problem. If the global searching schemes are taken, all the elements on the constraint

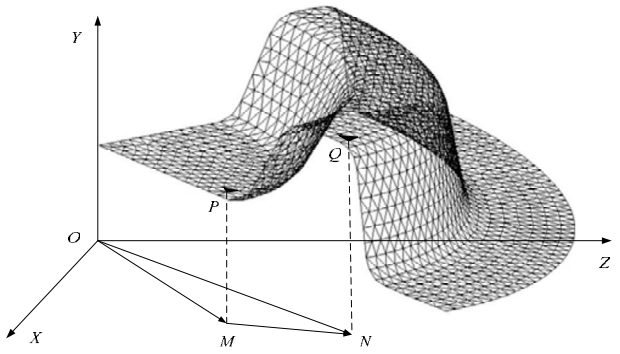


**Fig. 4 Walk-through algorithm to constrain the node movement**

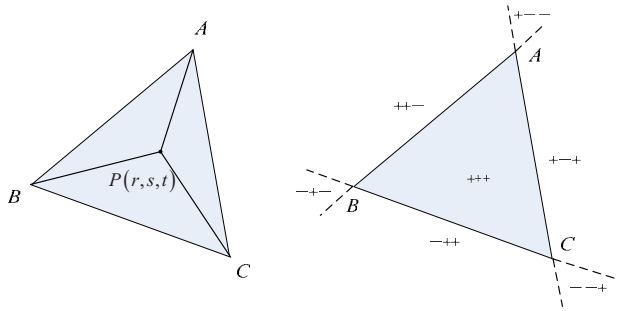


**Fig. 5 Barycentric coordinates and their signs: (*a*) point in a triangular and (*b*) signs of barycentric coordinates**

surface will be judged to enclose the node or not. The complexity of the method is $O(n)$ ($n$ is the element number). Actually, for a given node, only several elements have the possibility to be met with. If the number of element is small, this method could be acceptable. But for complex forming examples, fast and reliable searching scheme should be implemented. Point location is a fundamental problem in computational geometry. In order to simplify the problem, the mesh system of the current sliding constraint surface is projected vertically onto the $XOY$ plane to form another mesh. In this study, we present a point location algorithm, walk-through algorithm, to locate the point quickly (Fig. 5).

Walk-through methods solve point localization by walking a series of decisions to move into adjacent triangles judged closer to the query point [9]. The key element in walk-through algorithms is the decision step. A walk-through algorithm is based on traversing the triangulation using adjacency relation between triangles. The starting point is chosen to be any point already located in the triangulation; for instance a node. The decision to cross over to a neighboring triangle is determined by segment intersection test or by orientation test. Using barycentric coordinates to extract local information about the location of the query point allow a gradient descentlike walk toward the goal. The complexity of these single point location algorithm is $O(\sqrt{n})$ in $R^2$.

Consider a triangular element named $ABC$ (in counterclockwise (CCW) shown in Fig. 5) and the area of the triangle is defined as follows:

$$\Delta_{ABC} = \frac{1}{2}\begin{vmatrix} x_A - x_C & y_A - y_C \\ x_B - X_C & y_B - y_C \end{vmatrix} \tag{9}$$

Suppose if the nodes $A, B, C$ are CCW arranged, $\Delta_{ABC} > 0$, otherwise it is negative. The barycentric coordinates $(r,s,t)$ of point $P$ with respect to the triangle $ABC$ can be expressed by the ratio of two triangular areas.

$$r = \frac{\Delta_{PBC}}{\Delta_{ABC}}, \quad s = \frac{\Delta_{PCA}}{\Delta_{ABC}}, \quad t = \frac{\Delta_{PAB}}{\Delta_{ABC}} \tag{10}$$

where $r$, $s$ and $t$ satisfy the equation $r+s+t=1$.

For example, if the point $P$ locates on the right of directional edge $AB$, the sign of $r$ associated to edge $AB$ is negative (denoted as "–"), $r<0$. When $P$ lies on the left, $r$ is positive (denoted as "+"), $r>0$. If $P$ is on edge $AB$, $r=0$ (also denoted as "+"). Then we can conclude that if point $P$ is inside of the triangle element $ABC$, all barycentric coordinates are positive (denoted as "+++"). Any barycentric coordinate is positive means no possibility to go through the element. The case with all the signs negative "– – –" does not exist.

As shown in Fig. 6, the sign + indicate that the searching path "goes in" the triangular and the sigh – means that the searching path "goes out" of the triangle. The case (a) +++ means the end of the search because it has no more go out possibility. The case (b) "–++" and the case (c) "–+–" have both go in and go out possibilities to continue the searching paths. In case (c), searching path cross over to the neighboring triangle bordering the edge that represents the lowest of the barycentric coordinates. The procedure can be summarized below.

(1) Compute the barycentric coordinates $(r,s,t)$ of the query point $P$ with respect to the current triangle element $ABC$.
(2) Searching path walk through the edge that represents by the lowest of the barycentric coordinates. In case of Fig. 6($b$), $r(PBC)<0$, $s(PCA)>0$, and $t(PAB)>0$, cross over the edge $BC$.
(3) Stop when all the barycentric coordinates are positive, $r(PBC)>0$, $s(PCA)>0$, and $t(PAB)>0$.

**3.3 Constitutive Equations for Multistep FEM.** The traditional one-step inverse FEM, the stress-strain rate relation, which is derived from the associated flow rule and Hill's anisotropic yield criterion in plane stress, can be expressed as an integrated form [10].

$$f = \boldsymbol{\sigma}^{\mathrm{T}} \boldsymbol{P} \boldsymbol{\sigma} - \bar{\sigma}^2 = 0 \tag{11}$$

with $\boldsymbol{\sigma}^{\mathrm{T}} = \langle \sigma_x \ \sigma_y \ \sigma_{xy} \rangle$, where $\bar{\sigma}$ is the equivalent yield stress. The matrix $\boldsymbol{P}$ is in function of the mean anisotropic coefficient $\bar{r}$ obtained from the three anisotropic coefficients.

$$\boldsymbol{P} = \begin{bmatrix} 1 & -\dfrac{\bar{r}}{1+\bar{r}} & 0 \\ -\dfrac{\bar{r}}{1+\bar{r}} & 1 & 0 \\ 0 & 0 & \dfrac{2(1+2\bar{r})}{1+\bar{r}} \end{bmatrix}$$

$$\bar{r} = \frac{1}{4}(r_0 + 2r_{45} + r_{90}) \tag{12}$$

The proportional loading assumption allows obtaining the total plastic strains in terms of the total stresses.

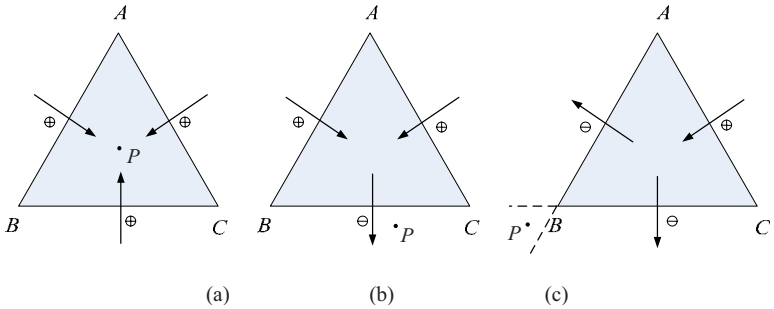


**Fig. 6 Walk-through algorithm based on barycentric coordinates**

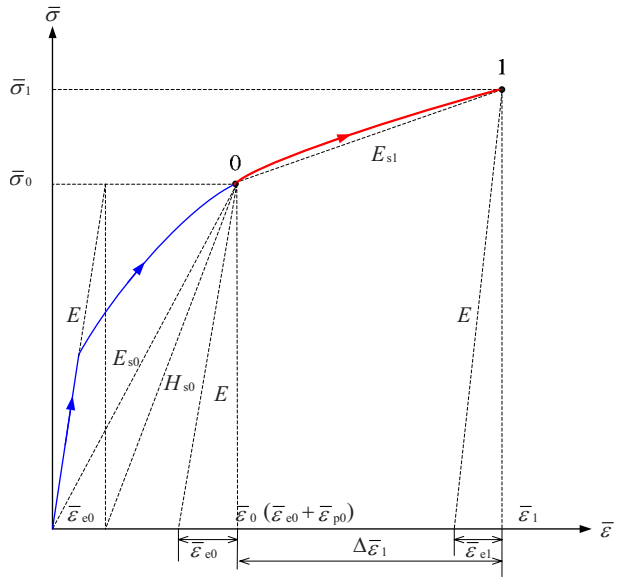


**Fig. 7 Uniaxial tress-strain curve for multistep forming process**

$$\boldsymbol{\varepsilon}_p = \frac{\bar{\varepsilon}_p}{\bar{\sigma}} \boldsymbol{P}\boldsymbol{\sigma} \tag{13}$$

with $\bar{\varepsilon}_p = (\boldsymbol{\varepsilon}_p^{\mathrm{T}} \boldsymbol{P}^{-1} \boldsymbol{\varepsilon}_p)^{1/2}$ the equivalent plastic strain.

If we assume the above anisotropy and incompressibility to be valid also for the small elastic deformation, then the Poisson coefficient is related to the mean anisotropy coefficient $\bar{r}$.

$$\nu = \frac{\bar{r}}{1+\bar{r}} \tag{14}$$

The total constitutive equation takes the following simple form:

$$\boldsymbol{\sigma} = E_s \boldsymbol{P}^{-1} \boldsymbol{\varepsilon} \tag{15}$$

where $E_s$ is the secant modulus of the uniaxial stress-strain curve

$$E_s = \frac{\bar{\sigma}}{\bar{\varepsilon}}; \quad \bar{\varepsilon} = (\boldsymbol{\varepsilon}^T \boldsymbol{P}^{-1} \boldsymbol{\varepsilon})^{1/2} \tag{16}$$

With the estimation of the total strains $\{\varepsilon\}$, we can compute $\bar{\varepsilon}$, $\bar{\sigma}$, and $E_s$, then estimate the stresses. This expression is fundamental for the stress-strain behavior in inverse FEM formulation for which a proportional loading form initial and final configurations has been assumed. This operation is performed for each numerical integration point through the thickness.

In the paper, some realistic intermediate configurations are introduced in the multistep inverse FEM to take into account the loading deformation paths. The Newton–Raphson iteration is conducted during all steps from the flat blank to the final workpiece. The first step is conducted between the initial solution of the flat blank and the first intermediate configuration restricted to the current sliding constraint surface. In each step, the lower configuration is noted as the initial state and the adjacent higher is noted as the final state. The procedure is more like that of flow theory of plasticity. In the incremental approaches, the stress increments are often calculated by an implicit algorithm of plastic integration, called return-mapping algorithm proposed by Simo and Taylor [11], but the plastic integration is very time consuming. In order to preserve the computational efficiency of inverse FEM, a pseudodeformation theory of plasticity based constitutive equation is proposed.

Figure 7 shows the uniaxial stress-strain curve for multistep forming process. In order to simplify the expression of multistep constitutive equations, only one intermediate configuration is introduced. The intermediate state "0" defined by the total strain $\boldsymbol{\varepsilon}_0$ is started from a zero plastic strain. Strain $\boldsymbol{\varepsilon}_0$ is composed of equivalent elastic strain $\bar{\varepsilon}_{e0}$ and equivalent plastic strain $\bar{\varepsilon}_{p0}$. The corresponding secant modulus is $E_{s0}$. State "1" defined by the total strain $\boldsymbol{\varepsilon}_1$ expresses the state of final workpiece. The corresponding equivalent elastic strain, equivalent plastic strain and secant modulus are noted as $\bar{\varepsilon}_{e1}$, $\bar{\varepsilon}_{p1}$, and $E_{s1}$, respectively. To find the middle stress state $\boldsymbol{\sigma}_0$, the traditional one-step inverse FEM can be carried out. Now, the question is: "Starting from the state 0, how to proceed to reach another state defined by $\boldsymbol{\varepsilon}_1$, assuming a proportional loading between states 0 and 1?"

For the continuity of deformation from flat blank to final workpiece, the secant modulus $E_{s1}$ can be obtained in a simple form based on Fig. 7.

$$E_{s1} = \frac{\bar{\sigma}_1 - \bar{\sigma}_0}{\bar{\varepsilon}_1 - \bar{\varepsilon}_0} = \frac{\bar{\sigma}(\bar{\varepsilon}_1) - \bar{\sigma}(\bar{\varepsilon}_0)}{\bar{\varepsilon}_1 - \bar{\varepsilon}_0} \tag{17}$$

Thus, the stress tensor of state 1 can be evaluated

$$\boldsymbol{\sigma}_1 = \boldsymbol{\sigma}_0 + E_{s1} \boldsymbol{P}^{-1} (\varepsilon_1 - \varepsilon_0) \tag{18}$$

To determine the stress and strain of state 1, the procedure can be summarized as follows:

(1) Compute the displacement, strain, and stress of state 0: $\boldsymbol{u}_0, \boldsymbol{\varepsilon}_0, \boldsymbol{\sigma}_0$.

(2) Compute displacement and strain increment

$$\Delta \boldsymbol{u}_1 = \boldsymbol{u}_1 - \boldsymbol{u}_0 \Delta \boldsymbol{\varepsilon}_1 = \boldsymbol{\varepsilon}_1 - \boldsymbol{\varepsilon}_0 \Delta \bar{\varepsilon}_1 = \bar{\varepsilon}_1 - \bar{\varepsilon}_0$$

(3) If $\bar{\sigma}_1 < \sigma_s$, the deformation is elastic, the stress increment can be expressed as

$$\Delta \boldsymbol{\sigma}_1 = \boldsymbol{D}_e \Delta \boldsymbol{\varepsilon}_1$$

where $\boldsymbol{D}_e$ is the elastic matrix.

(4) If $\bar{\sigma}_1 \geq \sigma_s$, the deformation is plastic, the stress increment is

$$\Delta \boldsymbol{\sigma}_1 = E_{s1} \boldsymbol{P}^{-1} \Delta \boldsymbol{\varepsilon}_1$$

where $\boldsymbol{P}$ is the anisotropic matrix defined by the average planar anisotropy.

(5) If $\Delta \bar{\varepsilon}_1 \geq 0$, it is a loading process. The stress tensor of state 1can be obtained

$$\boldsymbol{\sigma}_1 = \boldsymbol{\sigma}_0 + \Delta \boldsymbol{\sigma}_1 = \boldsymbol{\sigma}_0 + E_{s1} \boldsymbol{P}^{-1} \Delta \boldsymbol{\varepsilon}_1$$

(6) If $\Delta \bar{\varepsilon}_1 < 0$, it is a unloading process. The stress tensor of state 1 will become

$$\boldsymbol{\sigma}_1 = \boldsymbol{\sigma}_0 + \Delta \boldsymbol{\sigma}_1 = \boldsymbol{\sigma}_0 + \boldsymbol{D}_e \Delta \boldsymbol{\varepsilon}_1$$

The procedure will continue until the convergence criterion for the global iterations are achieved.

## 4 Implementation of Multistep Inverse FEM

The flowchart of multistep inverse FEM is shown in Fig. 8. In order to get the initial solutions on flat plane and all other constraint surfaces, area minimization algorithm, and node relocalization technique are implemented geometrically without considering the effect of process and material parameters on forming process. The Newton–Raphson iteration is conducted during all steps from the flat blank to the final workpiece. In step $n$, the lower configuration is noted as the initial state and the adjacent higher one is noted as the final state. After a converged iteration for the current step $n$, the position of nodes is updated in the initial state and strain and thickness distribution are updated in the final state. All the information on the final state becomes the preliminary initial state of step $n+1$. The iteration of each step is terminated until the displacement or residual force convergence criterion is satisfied.

$$\left\| \frac{\Delta U}{U} \right\|_2 \leq \varepsilon_D \tag{19}$$

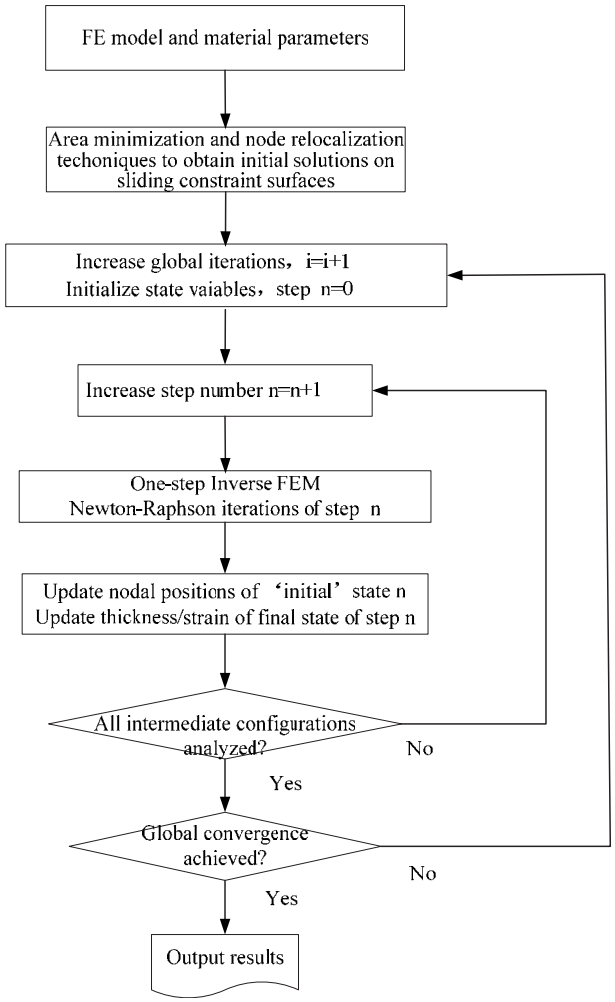


**Fig. 8 Flowchart of multistep inverse FEM**

$$\|R\|_2 \leq \varepsilon_F \tag{20}$$

where $\varepsilon_D$ and $\varepsilon_F$ are small positive value defined as $10^{-5}$ and $10^{-2}$, respectively.

The convergence criterion for the global iterations is

$$\frac{\sum_{n=1}^{\text{final step}} \|\Delta U\|_2}{\text{total no. of steps}} \leq \varepsilon_G \tag{21}$$

where $\varepsilon_G$ is defined between $10^{-1}$ and $10^{-2}$.

## 5 Numerical Validations

The presented algorithms described above have been implemented in a finite element code, INVERSTAMP, and applied to several examples of sheet metal stamping. In the paper, a two-step deep-drawing of cylinder cup and a three-step drawing S-rail are adopted to confirm the validity of the proposed developments.

**5.1 Two-Step Cylinder Cup Drawing.** The computer aided design (CAD) model and geometry of the final cup for benchmark test is illustrated in Fig. 9. The material properties and the process variables for the analysis of the cylinder cup drawing are as follows: stress-strain curve $\bar{\sigma}=729.09(0.01345+\bar{\varepsilon})^{0.1657}$ MPa, elastic modulus $E=200$ GPa, Poisson's ratio $\nu=0.3$, Lankford value $r=0.95$, initial sheet thickness $t_0=0.70$ mm, friction coefficient $\mu=0.13$, and blankholder force $F_b=15.0$ kN.

The model of the two-step deep-drawing cup is discretized by

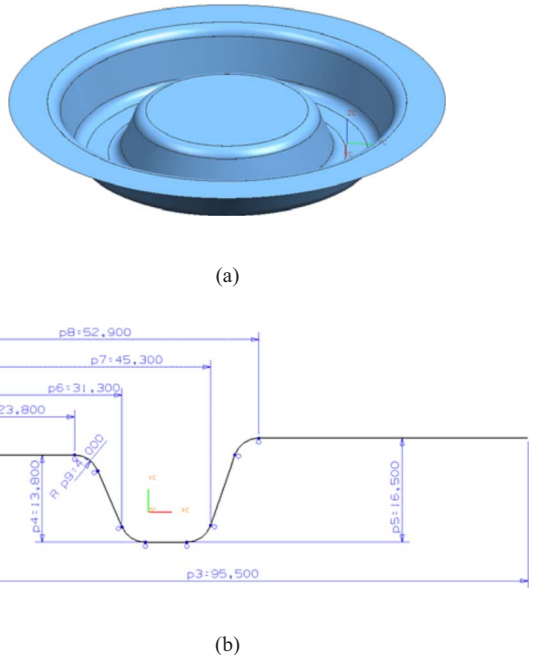


**Fig. 9 Two-step forming workpiece: (*a*) CAD modeling of final workpiece and (*b*) dimensions of half of the final workpiece**

9480 discrete Kirchhoff triangular (DKT) shell elements. Area minimization algorithm and node relocalization technique are carried out to get the intermediate configuration. The geometry of the current die face is discretized by 13,864 triangular elements and treated as sliding constraint surface. The mesh of initial flat blank was obtained with energy based algorithm proposed in Ref. [12].

Figures 10 show the thickness distribution obtained from two-step inverse analysis and incremental analysis. Figure 10(*a*) shows the thickness distribution of intermediate configuration with one-step inverse analysis method. The comparison shows well agreement between the two results. They both witness the thinning in the area around punch radius and thickening in the area under the binder. The maximum discrepancy in thickness distribution is about 0.03 mm. Figure 10(*b*) shows the thickness distribution for the final workpiece obtained from two-step inverse analysis and is compared with that of incremental analysis. The comparison demonstrates that the results of two-step inverse analysis are in better agreement with those of incremental analysis than those of one-step inverse analysis. However, the thickness distribution from two-step inverse analysis in the wall and flange region still disagree with that of incremental analysis, as shown in Fig. 10(*b*). The increment of the number of step is required to consider more accurate deformation path and the boundary conditions and improve the accuracy of the results from inverse analysis.

**5.2 Three-Step S-Rail Forming.** The CAD model and geometry of the S-rail is the same as Numisheet '96 [13]. The material properties and the process variables for the analysis of the S-rail forming are as follows: stress-strain curve $\bar{\sigma}=648(0.004+\bar{\varepsilon})^{0.220}$ MPa, elastic modulus $E=207$ GPa, Poisson's ratio $\nu=0.28$, Lankford value $r=1.65$, initial sheet thickness $t_0=0.80$ mm, friction coefficient $\mu=0.15$, and blankholder force $F_b=300$ kN.

Figures 11 and 12 show the configuration and location of die and punch with 10 mm and 20 mm drawing depth, respectively. The CAD model of punch and die are discretized with triangular meshes. With the proposed area minimization algorithm and node relocalization technique, the initial solutions of two intermediate configurations are obtained, shown in Figs. 13 and 14, and the sliding constraint surfaces are the die face, correspondingly. The

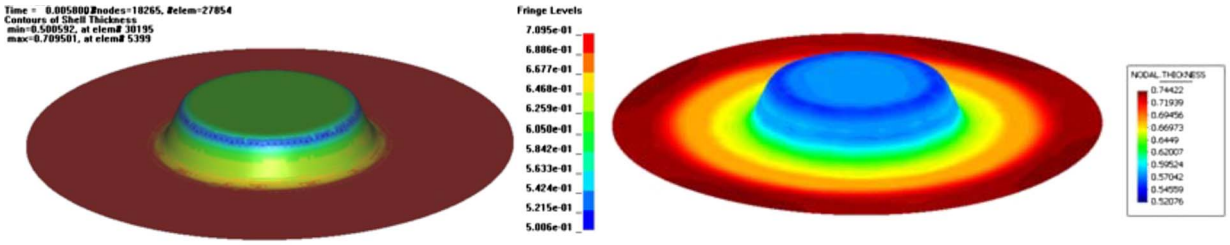


(a)

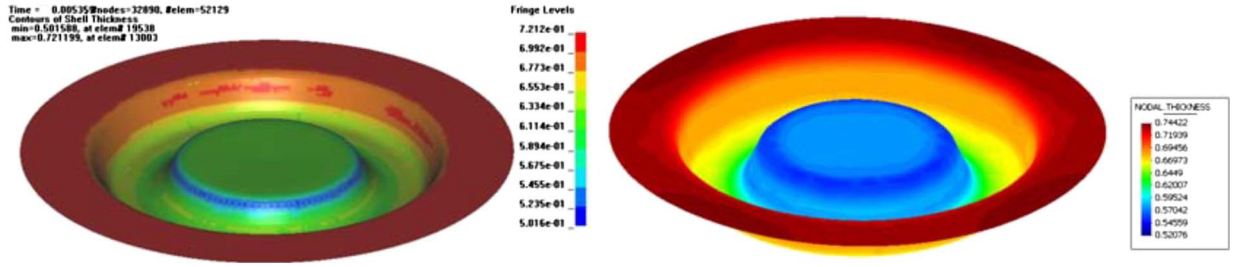


(b)

**Fig. 10 Comparisons of thickness distribution between proposed algorithm and incremental based FEM code: (*a*) from flat blank to intermediate sheet and (*b*) from flat blank to intermediate sheet and then final workpiece**

final workpiece is shown in Fig. 15 with 40 mm drawing depth. The figures demonstrate that the initial solutions are obtained adequately with the proposed algorithm although the punch geometry is very complicated with inclination of large angle.

In order to verify the reliability of the proposed developments, a direct elastic-plastic finite element analysis using LS-DYNA3D, one-step inverse FEM and multistep inverse FEM are used for comparison. According to our experience or the analysis results of LS-DYNA3D, sections AB and CD are the large deformation zones (Fig. 16). Predicting the thickness distribution along the two sections accurately will evaluate the effectiveness of the developments.

Because the LS-DYNA3D code is based on an updated Lagrangian formulation and a small increment method, it is a quite reliable simulation tool [14]. All the other calculated results are compared with those simulated with LS-DYNA3D. Figures 17 and 18 show the thickness distribution simulated by one-step /multistep inverse FEM and a direct elastic-plastic finite element analysis LS-DYNA3D. The figures indicate that although the tendencies of three curves are the same, the thickness obtained from

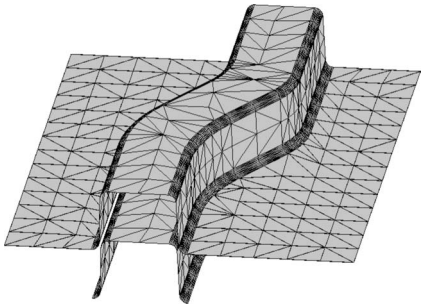

**Fig. 11 Tools location with 10 mm drawing depth**

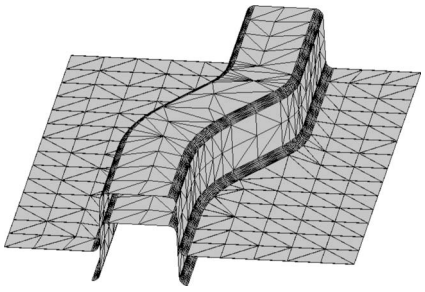

**Fig. 12 Tools location with 20 mm drawing depth**

**Fig. 13 Initial solution of intermediate configuration with 10 mm drawing depth**

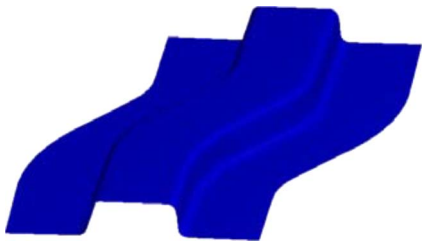

**Fig. 14 Initial solution of intermediate configuration with 20 mm drawing depth**

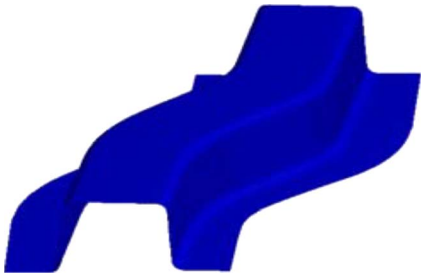

**Fig. 15 Final workpiece with 40 mm drawing depth**

multistep inverse analysis is closer to that of LS-DYNA3D than the one obtained from one-step inverse analysis. The maximum discrepancy of multistep inverse analysis compared with LS-DYNA3D is within 5% while the one of one-step inverse analysis exceed 10% to some extent.

## 6 Conclusion

A strategy of area minimization coupled with feasible sequential quadratic programming code is used to obtain initial intermediate configurations based on the known configurations of punch and die of the current step. An efficient walk-through point location algorithm is used to deal with contact searching problem and restrain the movement of corresponding nodes of intermediate configurations. A pseudodeformation theory of plasticity based constitutive equation is proposed, which can well reflect the actual forming condition such as elastic/plastic deformation or loading/unloading condition. Comparisons of numerical simulation results between the proposed multistep inverse FEM and LS-DYNA3D verify the feasibility of the proposed developments. Furthermore, the multistep inverse FEM is proved to be more accurate that one-step inverse FEM.

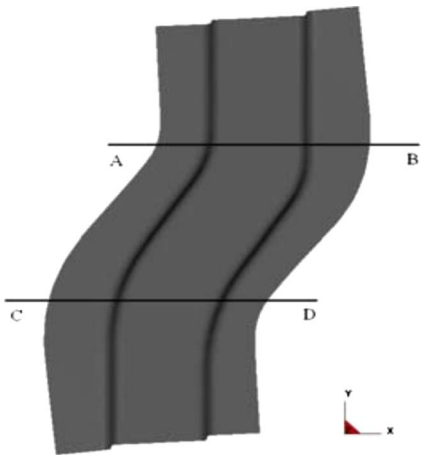


**Fig. 16 Contour of final workpiece with cutting sections AB and CD**

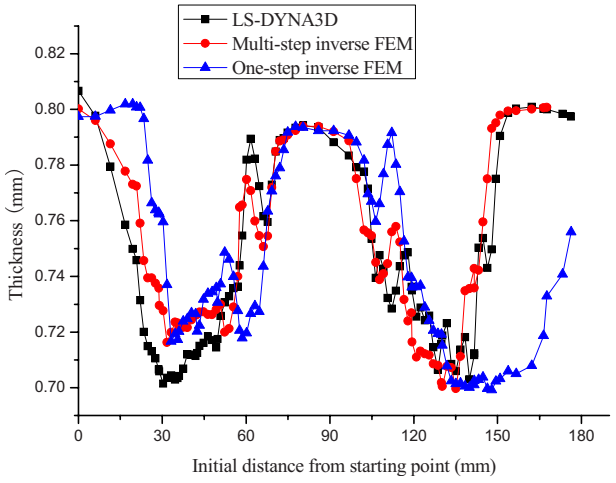


**Fig. 17 Comparison of thickness distribution (along AB section line)**

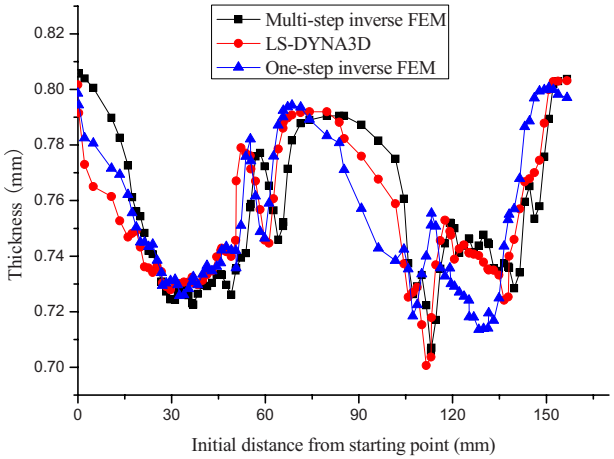


**Fig. 18 Comparison of thickness distribution (along CD section line)**


## Acknowledgment

The project was supported by the State Key Laboratory of Materials Processing and Die and Mold Technology, Huazhong University of Science and Technology (under Contract No. 09-15), by the Scientific Research Foundation for Outstanding Young Scientists of Shandong Province (under Contract No. BS2009ZZ011), and by the Science and Technology Program Foundation for Shandong Higher Education Institute (under Contract No. J09LD09).


## References


[1] Tekkaya, A. E., 2000, "State-of-the-Art of Simulation of Sheet Metal Forming," J. Mater. Process. Technol., **103**, pp. 14–22.

[2] Majlessi, S. A., and Lee, D., 1988, "Development of Multistage Sheet Metal Forming Analysis Method," J. Mater. Shaping Technol., **6**, pp. 41–54.

[3] Lee, C. H., and Cao, J., 2001, "Shell Element Formulation of Multi-Step Inverse Analysis for Axisymmetric Deep Drawing Process," Int. J. Numer. Methods Eng., **50**, pp. 681–706.

[4] Guo, Y. Q., Li, Y. M., Bogard, F., and Debray, K., 2004, "An Efficient Pseudo-Inverse Approach for Damage Modeling in the Sheet Forming Process," J. Mater. Process. Technol., **151**, pp. 88–97.

[5] Lee, C. H., and Huh, H., 1998, "Three Dimensional Multi-Step Inverse Analyses for the Optimum Blank Design in Sheet Metal Forming Processes," J. Mater. Process. Technol., **80–81**, pp. 76–82.

[6] Kim, S. H., and Huh, H., 2001, "Finite Element Inverse Analysis for the Design of Intermediate Dies in Multi-Stage Deep-Drawing Processes With Large Aspect Ratio," J. Mater. Process. Technol., **113**, pp. 779–785.

[7] Huang, Y., Chen, Y. P., and Du, R. X., 2006, "A New Approach to Solve Key Issues in Multi-Step Inverse FEM in Sheet Metal Stamping," Int. J. Mech. Sci., **48**, pp. 591–600.

[8] Tang, B., Zhao, Z., Chen, J., Dong, X., and RUAN, X., 2006, "Development of Multistage Sheet Metal Forming Simulation Based on Multi-Step Inverse Analysis Approach," Chin. J. Mech. Eng., **42**, pp. 211–217.

[9] Sundarewara, R., and Schrater, P., 2003, "Extensible Point Location Algorithm," Proceedings of the 2003 International Conference on Geometry Modeling and Graphics, London, UK.

[10] Naceur, H., Delamézière, A., Batoz, J. L., Guo, Y. Q., and Knopf-Lenoir, C., 2004, "Some Improvements on the Optimum Process Design in Deep Drawing Using the Inverse Approach," J. Mater. Process. Technol., **146**, pp. 250–262.
[11] Simo, J. C., and Taylor, R. L., 1986, "A Return-Mapping Algorithm for Plane Stress Elasto-Plasticity," Int. J. Numer. Methods Eng., **22**, pp. 649–670.
[12] Tang, B. T., Zhao, Z., Hagenah, H., and Lu, X. Y., 2007, "Energy Based Algorithms to Solve Initial Solution in One-Step Finite Element Method of Sheet Metal Stamping," Comput. Methods Appl. Mech. Eng., **196**, pp. 2187–2196.
[13] Duarte, J. F., and Rocha, A. B., 1996, "A Brief Description of an S-Rail Benchmark," J. K. Lee, G. L. Kinzel, and R. H. Wagoner, eds., Proceedings of Numisheet '96, Ohio State University, pp. 336–433.
[14] Hallquist, J. O., 1998, LS-DYNA Theoretical Manual [CP]. Livermore Software Technology Corporation.